nature nanotechnology

Review article

https://doi.org/10.1038/s41565-024-01704-3

Understanding epitaxial growth of two-dimensional materials and their homostructures

Received: 3 April 2023

Accepted: 22 May 2024

Published online: 10 July 2024

Check for updates

Can Liu[1,2,8], Tianyao Liu[1,8], Zhibin Zhang[1,8], Zhipei Sun[3], Guangyu Zhang[4,5], Enge Wang[4,6] & Kaihui Liu[1,4,7]

The exceptional physical properties of two-dimensional (2D) van der Waals (vdW) materials have been extensively researched, driving advances in material synthesis. Epitaxial growth, a prominent synthesis strategy, enables the production of large-area, high-quality 2D films compatible with advanced integrated circuits. Typical 2D single crystals, such as graphene, transition metal dichalcogenides and hexagonal boron nitride, have been epitaxially grown at a wafer scale. A systematic summary is required to offer strategic guidance for the epitaxy of emerging 2D materials. Here we focus on the epitaxy methodologies for 2D vdW materials in two directions: the growth of in-plane single-crystal monolayers and the fabrication of out-of-plane homostructures. We first discuss nucleation control of a single domain and orientation control over multiple domains to achieve large-scale single-crystal monolayers. We analyse the defect levels and measures of crystalline quality of typical 2D vdW materials with various epitaxial growth techniques. We then outline technical routes for the growth of homogeneous multilayers and twisted homostructures. We further summarize the current strategies to guide future efforts in optimizing on-demand fabrication of 2D vdW materials, as well as subsequent device manufacturing for their industrial applications.

Over the past two decades, the family of two-dimensional (2D) materials has markedly expanded and now includes nearly 2,000 theoretically predicted and hundreds of laboratory-accessible species[1]. This evolution is closely connected to the advancements in material fabrication technologies. Mechanical exfoliation from bulk crystals plays a pioneering role in the discovery and isolation of graphene and yields high-quality materials, but faces challenges in large-scale production. Alternative solution-based exfoliation methods offer scalability of 2D materials but they may introduce defects, impurities and even chemical modifications. Epitaxial growth techniques, however, stand out by allowing the assembly of atoms or molecules into 2D materials on various substrates without lattice-matching requirements and providing precise control over composition and crystallinity, showcasing the potential for fabricating large-area, high-quality, single-crystal films.

The concept of 2D-material epitaxy dates back to the 1960s, when John May identified unassigned low-energy electron diffraction

[1]State Key Laboratory for Mesoscopic Physics, Frontiers Science Center for Nano-optoelectronics, School of Physics, Peking University, Beijing, China. [2]Key Laboratory of Quantum State Construction and Manipulation (Ministry of Education), Department of Physics, Renmin University of China, Beijing, China. [3]Department of Electronics and Nanoengineering, Quantum Technology Finland Centre of Excellence, Aalto University, Espoo, Finland. [4]Songshan Lake Materials Laboratory, Institute of Physics, Chinese Academy of Sciences, Dongguan, China. [5]Beijing National Laboratory for Condensed Matter Physics, Institute of Physics, Chinese Academy of Sciences, Beijing, China. [6]International Center for Quantum Materials, Collaborative Innovation Center of Quantum Matter, Peking University, Beijing, China. [7]Interdisciplinary Institute of Light-Element Quantum Materials and Research Center for Light-Element Advanced Materials, Peking University, Beijing, China. [8]These authors contributed equally: Can Liu, Tianyao Liu, Zhibin Zhang.
e-mail: khliu@pku.edu.cn

https://doi.org/10.1038/s41565-024-01704-3

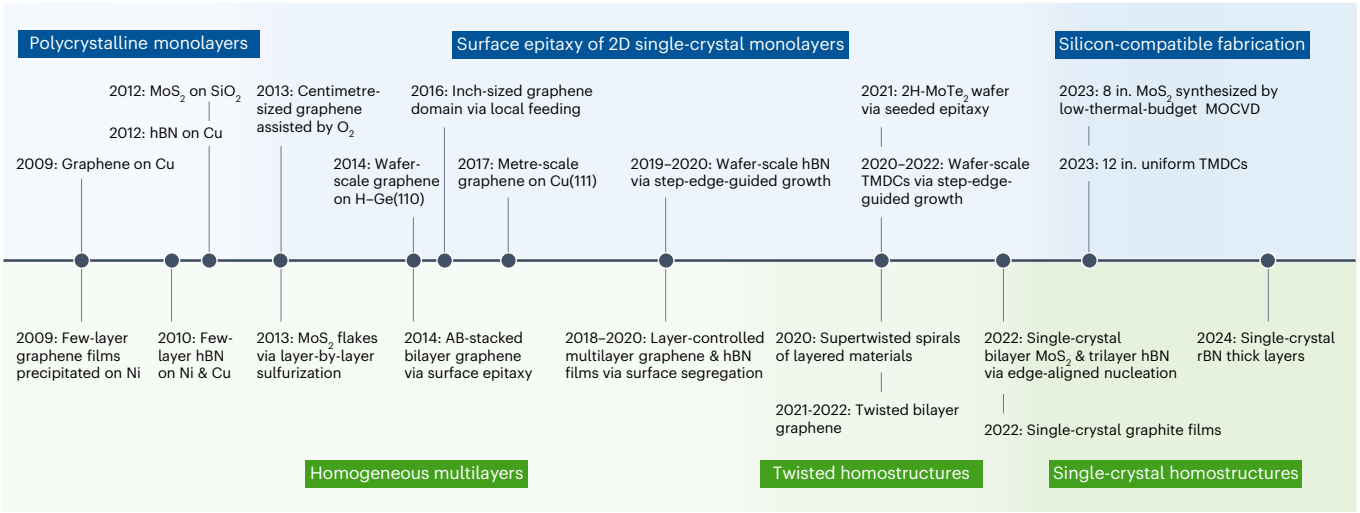

Fig. 1 | Representative progress in the epitaxial growth of characteristic 2D vdW materials and their homostructures. Graphene on Cu[4], MoS_2 on SiO_2[143], hBN on Cu[144], centimetre-sized graphene assisted by oxygen[28], wafer-scale graphene on H–Ge(110)[46], inch-sized graphene domain via local feeding[38], metre-scale graphene on Cu(111)[6], wafer-scale hBN via step-edge-guided growth[7,55], 2H-$MoTe_2$ wafer via seeded epitaxy[10], wafer-scale TMDCs via step-edge-guided growth[9,56,57], 8 in. MoS_2 synthesized by low-thermal-budget metal–organic CVD (MOCVD)[145], 12 in. uniform TMDCs[75,134], few-layer graphene films precipitated on Ni[146], few-layer hBN on Ni[147], few-layer hBN on Cu[148], MoS_2 flakes via layer-by-layer sulfurization[149], AB-stacked bilayer graphene via surface epitaxy[150], layer-controlled multilayer graphene films via surface segregation[99,103,104], layer-controlled multilayer hBN films via surface segregation[107,151], supertwisted spirals of layered materials[129], twisted bilayer graphene[12,126], single-crystal bilayer MoS_2 via edge-aligned nucleation[97], single-crystal trilayer hBN via edge-aligned nucleation[98], single-crystal graphite films[109], single-crystal rBN thick layers[14].

patterns on high-temperature metal substrates in hydrocarbons and attributed them to the growth of 'monolayer graphite'[2]. The term 'van der Waals (vdW) epitaxy' was introduced by Koma et al. in 1984 for the fabrication of subnanometre $NbSe_2$ films on cleaved MoS_2 surfaces[3]. Initially, these explorations remained confined within the surface physics community and did not attract broader attention. The field has undergone a transformation over the past two decades, beginning with the discovery and isolation of graphene in 2004, which motivated a series of breakthrough 'waves' in the exploration and epitaxial growth of characteristic 2D vdW materials and their homostructures (Fig. 1). The synthesis of monolayer graphene on copper foil in 2009 set the first wave in motion, with the epitaxy mechanisms being deciphered over the following decade, promoting the industrial production of single-crystal films[4–6]. Subsequent waves were attributable to the epitaxy of 2D hexagonal boron nitride (hBN) and transition metal dichalcogenides (TMDCs), achieving inch-sized single crystals very recently[7–10]. Emerging phenomena such as twistronics and moiré photonics in artificial multilayer systems have propelled another wave for the direct growth of out-of-plane homostructures with controlled stacking and twist angles[11–14]. Treading into the future, new waves of emerging 2D-material epitaxy potentially include monoelemental species (for example, black phosphorus, borophene and tellurene), non-transition-metal chalcogenides (for example, In_2Se_3, GeSe and Bi_2Se_3), 2D borides, carbides, nitrides, oxides, hydroxides and halides[15–18]. Although each wave has its own unique challenges, a universal epitaxy principle is underlying and essential for navigating these advancements.

This Review primarily focuses on the state-of-the-art technical routes in 2D vdW material epitaxial growth, exploring the basic principles and technical routes for domain nucleation, lateral expansion and vertical construction. It is divided into three main sections. In the first section, we discuss the current status of 2D single-crystal monolayer epitaxy along the in-plane direction, including the nucleation control of a single domain, orientation control of multiple domains, and quality control addressing defects. In the second section, we delve into the critical scientific questions, strategies and progress in the growth of 2D materials along the out-of-plane direction, including the fabrication of homogeneous multilayers and twisted homostructures. Finally, we provide a summary and outlook on the strategic directions of epitaxial growth and suggestions to guide the development of emerging 2D materials.

Growth of in-plane single-crystal monolayers

Nucleation control of a single domain

In general, the growth of 2D materials can be traced back to their initial nucleation. After feedstocks are introduced into the growth system, they reach a dynamic balance between adsorption and desorption from the substrate surface. Simultaneously, these feedstocks decompose into active species and then cluster at certain sites on the substrate, leading to the formation of zero-dimensional nucleation seeds. These nuclei gradually evolve into single-crystal domains by adatom attachment and bonding at one-dimensional (1D) edges, which usually occurs in a systematic and swift manner until domain coalescence (Fig. 2a). Therefore, controlling the nucleation of a single domain is fundamental to the epitaxial growth of 2D materials.

The nucleation of 2D atomic layered materials commonly occurs at active sites with high surface energy, including atomic steps, grain boundaries, defects and impurities on substrate surfaces[19]. However, the initial nuclei tend to be randomly distributed and oriented, forming polycrystals with numerous grain boundaries during their coalescence (Fig. 2b). Hence, suppressing nucleation by reducing the number of active sites on substrates has been proposed as a feasible and universal strategy for producing large-scale single-crystal films (Fig. 2c). Several pretreatment methods for metal substrates have been developed to enhance the smoothness and cleanliness of metal surfaces to eliminate active sites, such as surface rinsing or polishing[20,21], prolonged high-temperature annealing[22,23] and tailoring substrates such as folding copper 'enclosures'[24,25], showing remarkable inhibitory effects on the nucleation of graphene or hBN. Novel liquid-state substrates, including liquid gallium, indium, nickel, tin, gold and molten glass, have been employed to further improve surface flatness and promote the lateral growth of large-size domains[26,27]. Alternatively, the introduction of passivators such as oxygen[28], melamine[29] and hydroxylation[30] to preoccupy the active sites, or etchants such as hydrogen[31], water

https://doi.org/10.1038/s41565-024-01704-3

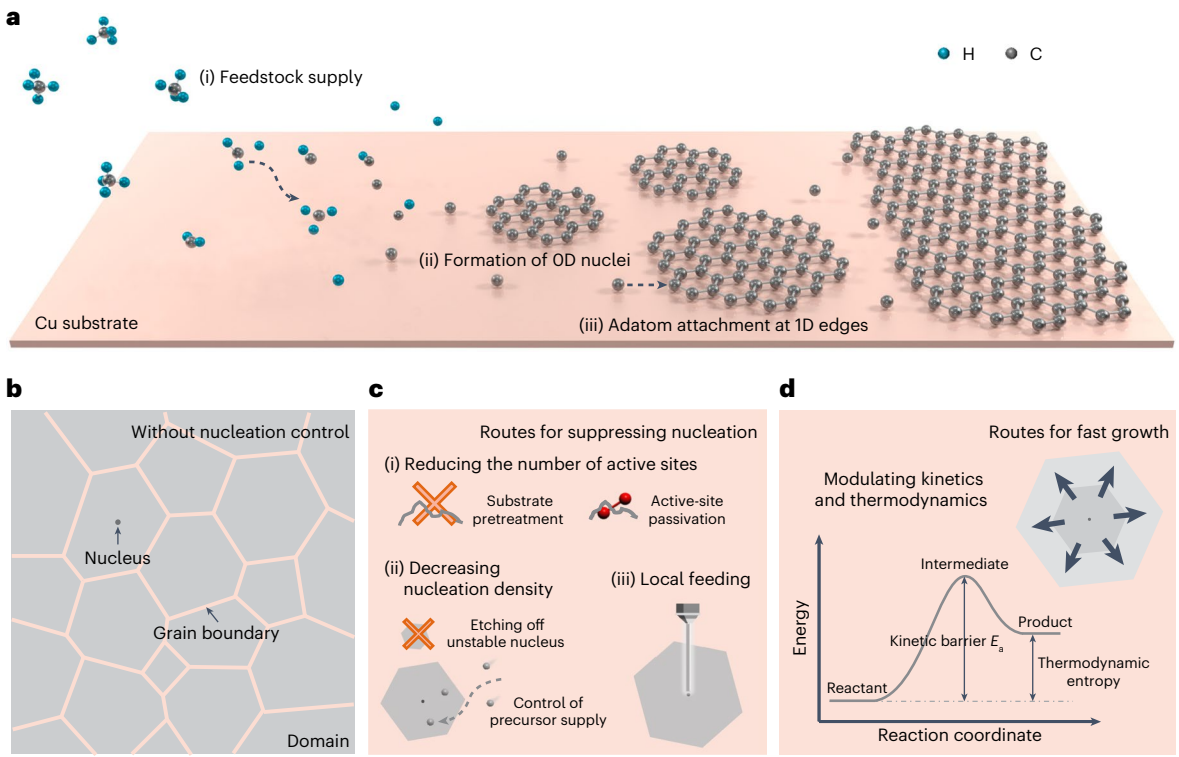

Fig. 2 | Nucleation control of a single domain. a, Growth process of graphene on a Cu substrate, including (i) supply of feedstocks, (ii) formation of zero-dimensional (0D) nuclei and (iii) adatom attachment at 1D edges. **b**, Formation of grain boundaries during the coalescence of domains without nucleation control. **c**, Routes for suppressing nucleation, including (i) reducing the number of active sites, (ii) decreasing nucleation density and (iii) local feeding. **d**, Routes for fast growth by modulating kinetics and thermodynamics.

vapour[32] and oxygen[33] to etch off the unstable nuclei, have enabled the expansion of individual graphene domains to centimetre scale and hBN domains to millimetre scale. The epitaxy of TMDCs necessitates precise control over the multielement supply; thus, their nucleation is highly dependent on the precursor stoichiometry and diffusion. Methods such as modulating the introduction time and the flow rate of precursors[34], and designing a diffusion barrier[35], a confined space[36] or a self-capping layer[37], have demonstrated comparable efficacy in decreasing the nucleation density and promoting diffusion for growing millimetre-scale TMDC domains.

The limit to suppressing nucleation is to control a single nucleus to evolve into a large-scale domain (Fig. 2c). Specialized local feeding techniques have been formulated to ensure the nucleation and growth of a single nucleus at predefined positions[38]. By pulling the polycrystalline substrates at the desired speed during local feeding, foot-long single-crystal graphene films can be synthesized through an evolutionary 'self-selection' of the fastest-growing domain orientation[39]. Moreover, implanting small single-crystal seeds onto other-phase polycrystalline films can trigger a solid-to-solid phase transition and recrystallization process, directing a wafer-scale lateral extension of 2H-$MoTe_2$ single crystals[10].

In addition to the reduction in the nucleation density, the acceleration of the source atom attachment at the 1D edge is equally important, since the fast growth of the domains can further reduce the nucleation at other sites, leading to higher single-crystal coverage in a shorter timeframe (Fig. 2d). This chemical reaction rate is determined by the kinetic processes and can be represented by the Arrhenius equation $k = A\exp(-E_a/RT)$, where k is the reaction rate constant, A is the pre-exponential factor, E_a is the apparent activation energy, R is the gas constant and T is the reaction temperature. On the basis of this equation, it was found early on that elevating the growth temperature could facilitate the rapid growth of domains to some extent[40]. Lowering the reaction barrier E_a by employing a catalyst for precursor decomposition can also greatly accelerate the growth rate k (ref. 38). Moreover, introducing foreign species such as fluorine to modulate the kinetics and thermodynamics of graphene growth has increased the growth rate to 200 μm s^{-1} (ref. 41).

The evolution of a single nucleus into a single-crystal domain involves two essential steps, including the formation of zero-dimensional nuclei and the adatom attachment at 1D edges. By reducing the nucleation density and accelerating the growth rate, the nucleation control of a single domain exhibits high repeatability and compatibility, effectively avoiding the formation of grain boundaries from multidomain stitching and rapidly fabricating large single-crystal domains. However, the typical size of individual 2D domains is merely in the range of micrometres to centimetres. Therefore, the coordinated modulation of multidomain orientations is inherently indispensable for producing larger-scale 2D single crystals.

Orientation control of multiple domains

On the basis of the control of individual domains, the stitching of multiple domains is crucial for the further formation of large-scale monolayer films. However, these domains tend to be randomly oriented on the substrate surface, resulting in polycrystalline films with high-density grain boundaries. These line defects can substantially impair the electronic performance, causing reduced carrier mobility and increased sheet and contact resistances, and hindering the development of high-performance devices[42]. In contrast, single-crystal 2D films can avoid the performance degradation originating from these defects and further ensure device-to-device consistency during integration. A feasible approach to producing large-size single-crystal films involves seamlessly stitching numerous domains by modulating their unidirectional alignment during the nucleation stage. In this regard, the interactions between the 2D materials and substrates offer

https://doi.org/10.1038/s41565-024-01704-3

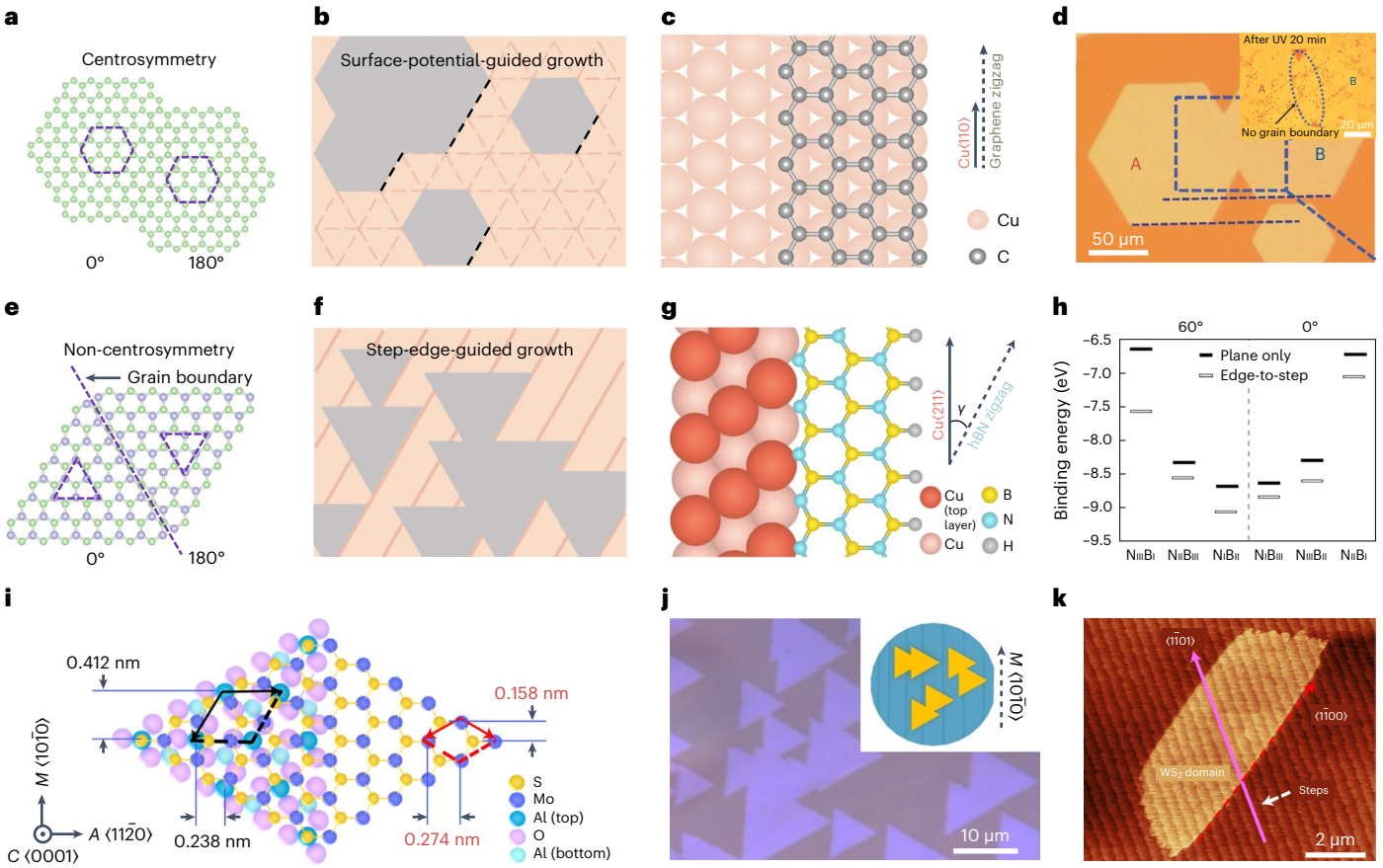

Fig. 3 | Orientation control of multiple domains. a, Schematic of the epitaxy of centrosymmetric 2D materials. The antiparallel domains (0° and 180°) are seamlessly stitched together without grain boundaries. **b**, Schematic for the growth of unidirectionally aligned domains guided by a periodic surface potential. **c**, Schematic of graphene grown on a Cu(111) substrate with a zigzag edge aligned along the Cu⟨110⟩ direction. **d**, Aligned graphene domains grown on Cu(111). Inset: no grain boundaries appeared after irradiation with ultraviolet (UV) light. **e**, Schematic of the epitaxy of non-centrosymmetric 2D materials. Twin grain boundaries are formed during the coalescence of antiparallel domains. **f**, Schematic for the growth of unidirectionally aligned domains guided by step edges. **g**, Schematic of hBN grown on a Cu(110) substrate with a zigzag edge coupled with a Cu⟨211⟩ step edge. **h**, Calculated bonding energies for the six hBN configurations on Cu(111), with and without consideration of the step-edge-guiding effect. The degeneracy of the two antiparallel configurations is disrupted by an energy difference of approximately 0.23 eV with Cu step edges. **i**, Schematic of the epitaxial relationship of MoS_2 on a sapphire (0001) substrate. **j**, Aligned MoS_2 domains grown on C/A sapphire (0001). Inset: schematic for the epitaxial alignment of MoS_2 domains to ⟨10$\bar{1}$0⟩ steps. **k**, A WS_2 domain grown on *a*-plane sapphire with a zigzag edge along the ⟨1$\bar{1}$00⟩ direction via the combination of vdW and step interactions between 2D domains and substrates. Panels adapted with permission from: **d**, ref. 45, Wiley; **h**, ref. 55, Springer Nature Limited; **i**,**j**, ref. 9, Springer Nature Limited; **k**, ref. 57, Springer Nature Limited. Panel **g** reproduced with permission from ref. 7, Springer Nature Limited.

a potential solution, as substrate surface symmetry plays a crucial role in determining the arrangement of the discrete domains.

In centrosymmetric 2D materials, domains possessing 0°- and 180°-rotated orientations exhibit substantial equivalence, enabling their seamless coalescence without grain boundaries during growth (Fig. 3a). The periodic surface potential of substrates has proven effective in guiding the unidirectional epitaxy of these centrosymmetric 2D materials, where the orientation of the 2D domains is primarily determined by the surface lattice symmetry of the substrate (Fig. 3b). For six-fold symmetric graphene, the hexagonal close-packed lattice of Cu(111) is considered an ideal surface for growing single-crystal films[43]. Generally, the graphene zigzag edges align along the Cu⟨110⟩ direction, consequently guiding graphene domains in a consistent direction on Cu(111) substrates[44] (Fig. 3c). The seamless stitching of the adjacent graphene domains can be verified through grain-boundary visualization techniques, with no discernible cracks exposed at the domain junctions[45] (Fig. 3d). Two-fold symmetric Cu(110) and Ge(110) surfaces have also been demonstrated to have a suitable symmetric relationship with the graphene lattice, allowing well aligned nucleation of multiple graphene domains[44,46]. On the basis of the seamless merging of multiple domains with perfect unidirectional alignment, single-crystal 2D films can be synthesized, and their maximum dimensions are basically limited by the size of the single-crystal substrate. Inspired by this notion, various annealing techniques, including repeated annealing upon polishing[45], contact-free annealing[47], temperature-gradient-driven annealing[6] and magnetron sputtering techniques[48,49], have been developed to prepare large-scale single-crystal Cu(111). Graphene domains epitaxially grown on these substrates exhibit high orientation and eventually merge into metre-scale single-crystal graphene films.

For non-centrosymmetric 2D materials, domains featuring 0°- and 180°-rotated orientations exhibit energetic degeneracy when epitaxially grown on centrosymmetric substrates. This generally results in an equal likelihood of antiparallel domain nucleation, causing the inevitable formation of undesired twin boundaries when two domains merge[50,51] (Fig. 3e). This issue has consistently posed a challenge during the preparation of non-centrosymmetric 2D single crystals. For hBN, employing low-symmetry Cu(102) and Cu(103) substrates has proven effective in guiding their domains towards a preferred orientation with over 97% alignment[52]. Stepped surfaces on specific substrates are recognized to be effective in guiding the unidirectional alignment of

domains (Fig. 3f). Some index planes of metal substrates inherently possess terraces and atomic steps[7], whose directions are primarily determined by the crystallographic orientation and surface symmetry. Additionally, miscutting ingots at specific angles can also construct a regular stepped surface morphology after thermal reconstruction, and the step alignment direction, spacing and height can be modulated by the miscut angle and annealing temperature[53,54]. Two-fold symmetric Cu(110) substrates, with naturally parallel Cu⟨211⟩ atomic steps on their vicinal surfaces, can disrupt the nucleation equivalency of antiparallel hBN domains due to the strong coupling between the ⟨211⟩ step edges and hBN zigzag edges[7] (Fig. 3g). Therefore, unidirectional nucleation occurs and facilitates highly aligned domains with a consistency exceeding 99%, producing a decimetre-scale single-crystal hBN monolayer. Furthermore, this step-edge-guided growth mechanism exhibits broad applicability and high repeatability across various crystal facets, as evidenced by the unique alignment of hBN domains on Cu(410) substrates. Even on a highly symmetric substrate, it is also feasible to employ step edges to decrease surface symmetry and align the domains via this step-edge-guided route. For instance, the spontaneously present top-layer Cu step edges on the centrosymmetric Cu(111) substrate can disrupt the degeneracy of the two hBN configurations by a binding energy difference of approximately 0.23 eV (Fig. 3h), enabling the successful synthesis of wafer-scale single-crystal hBN monolayers[55].

The step-edge-guided route has also been developed as a versatile and scalable approach for fabricating other non-centrosymmetric 2D single crystals beyond hBN, with TMDCs routinely employing this strategy. The Au⟨110⟩ steps on Au(111) surfaces have demonstrated their effectiveness in modulating domain alignment, increasing the orientation consistency of MoS_2 domains to an impressive 98% (ref. 56). Beyond metal substrates, the atomic steps engineered on sapphire substrates can also break the nucleation energy degeneracy of the antiparallel domains, thereby promoting the oriented growth of 2D films on insulating substrates for high-performance electronic devices. By intentionally miscutting the *c*-plane sapphire towards its *A* axis, surface steps along the ⟨10$\bar{1}$0⟩ direction are generated. The epitaxial relationship triggers the alignment of the zigzag edges of triangular TMDC domains with these ⟨10$\bar{1}$0⟩ steps, inhibiting the formation of antiparallel domains and guiding the epitaxy of uniform 2 in. MoS_2 and $MoSe_2$ single crystals[9] (Fig. 3i,j). The combination of vdW and step interactions between 2D domains and insulating substrates can disrupt energy degeneracy as well, enabling the fabrication of wafer-scale WS_2 single crystals on *a*-plane sapphire[57] (Fig. 3k). Moreover, a high ratio of S/Mo precursors has been designed for mediating the MoS_2 domains to nucleate along step edges of sapphire substrates and then rotate to align with the substrate lattice, inducing the evolution of unidirectionally aligned MoS_2 triangular crystals[58]. Notably, even in the case of heteroepitaxial growth of layered materials with giant out-of-plane lattice mismatches, the uniform alignment of crystal domains can also be guided by the step edges, as evidenced by the step-climbing epitaxy of Bi_2O_2Se single-crystal films on $SrTiO_3$ substrates[59].

However, the step edges may not direct the epitaxy when the nucleation kinetically prefers the terraces rather than the step edges in some growth cases of high temperature or low deposition rate[60]. The simultaneous formation of the grain nuclei and substrate steps has been revealed as a robust mechanism to ensure the initial nucleation near the immature step edges, thereby achieving the universal single-crystal epitaxy of TMDCs, including MoS_2, NbS_2, WSe_2 and $NbSe_2$[61]. The preferred orientation of the WSe_2 domains can be effectively switched between 0° and 60° when they nucleate at the top and bottom edges of sapphire steps, respectively[62]. Nonetheless, a recent study indicated that step-edge guidance was potentially not necessary for single-crystal epitaxy, since the growth of mono-oriented TMDC domains could be guaranteed by reconstructing the surfaces of *c*-plane sapphire substrates to expose a single-type slab surface, without the aid of the step edges[54].

Large-scale 2D single-crystal monolayers can be fabricated by manipulating the unidirectional alignment of multiple domains. On the basis of this principle, the domain orientations of centrosymmetric 2D materials can be guided by the periodic potentials on symmetrically matched substrates, while the domain orientations of non-centrosymmetric 2D materials can be efficiently controlled by a step-edge-guided mechanism. Currently, the epitaxy of typical 2D vdW single crystals has progressed through these strategies. Material epitaxy employing techniques such as chemical vapour deposition (CVD), molecular beam epitaxy or metal–organic CVD has promise for expansion along this path to create high-quality single crystals of emerging 2D materials[63].

Quality control addressing defects

The unidirectional alignment of multiple domains plays a pivotal role in eliminating the grain boundaries and fostering the formation of large 2D single crystals. However, atomic defects attributable to the exposed surface characteristics of the 2D materials persist within these crystals. Such defects invariably scatter charge carriers and phonons, resulting in a reduced ballistic transport path length and negatively impacting the electrical properties. Therefore, addressing these defects becomes a critical step in further enhancing the quality and performance of 2D single crystals.

Many studies have reported the successful synthesis of high-quality 2D materials, as primarily evidenced through transport and optical analyses[64]. Currently, the quality of the CVD-grown graphene films has reached competitive levels with high field-effect mobilities of 7,000–30,000 $cm^2\ V^{-1}\ s^{-1}$, approaching the values of exfoliated flakes from geologic crystals and theoretical limits[28,65,66]. A more direct and quantitative investigation of the point defects relies on high-resolution characterization techniques such as scanning transmission electron microscopy and scanning tunnelling microscopy[67,68]. On the basis of these techniques, various atomic-scale defects in TMDCs have been observed, including vacancies with the chalcogen (X) atoms, transition metal (M) atoms and MX_n clusters absent, antisite defects with mutually substituted M or X atoms, and other foreign atoms mixed into the lattice[69]. Among them, the dominant point defects in CVD-grown TMDCs have been identified as the chalcogen vacancies, with densities of the order of 10^{12}–$10^{13}\ cm^{-2}$ (refs. 9,70,71). To reduce these vacancies, alternative precursors such as sulphur-containing thiol solution and hydroxide W species have been employed to provide an energetically favourable route for the chalcogenization process in the TMDC growth, reducing the defect density by approximately an order of magnitude[72,73]. In addition, a chalcogen monomer supply method has been developed as a defect-healing strategy to achieve stoichiometric TMDC films[74,75]. Once these active monomers traverse the vicinity of a vacancy during growth, the unsaturated bonds can readily capture and accommodate them, subsequently allowing for an atomic-level defect repair via an exothermic reaction.

The structural defects in synthetic 2D materials can be further repaired and reduced via post-treatment methods[64]. The etching–regrowth approach has emerged as a promising strategy for eliminating crystalline defects[76,77]. This process involves selective etching of defect sites and subsequent growth to reconstruct 2D-material structures with perfect atomic arrangements, much like patching a piece of fabric. To date, this strategy has proven effective in the fabrication of near-defect-free graphene films[31], basically satisfying the standards set for most industrial applications. Besides, an additional post-growth annealing process can also effectively heal defective sites, as evidenced by the two-orders-of-magnitude improvement in the conductivity of graphene sheets after annealing in an ethylene atmosphere[78]. Similarly, chalcogen vacancies in TMDCs can be significantly healed towards intrinsic charge transport by thiol chemistry[79] and chalcogen gas annealing[80]. Moreover, the advent of precise in situ technologies, including the direct manipulation of individual atoms at

https://doi.org/10.1038/s41565-024-01704-3

Table 1 | Current defect levels of typical 2D vdW materials

2D materials	Synthetic route	Point defect density ($\times 10^{12}$ cm^{-2})	Mobility at room temperature (cm^2 V^{-1} s^{-1})
Graphene	CVD[135]	V_{total} ~2×10^{-2}	—
	CVD[136]	V_{total} ~4.2×10^{-2}	—
	Exfoliated[137]	V_{total} ~10^{-3}–10^{-2}	—
	Etching–regrowth treated[31]	—	13,000
MoS_2	CVD[9]	V_S ~9	102.6
	CVD[67]	V_S ~13	11
	CVD[74]	V_S ~2	42
	Exfoliated[67]	V_S ~11	—
	Exfoliated[138]	V_S ~37	7.7
	PVD[67]	V_{an} ~28	0.5
	PLD[139]	V_S ~38	—
	MOCVD[140]	V_S ~27	4.0
	Thiol-annealing treated[79]	V_S ~16	81
WS_2	CVD[73]	V_{total} ~21	17
	Hydroxide vapour deposition[73]	V_{total} ~2.5	198
WSe_2	CVD[70]	V_{Se} ~16	—
	CVD[71]	V_{Se} ~53	1.2
	MBE[141]	V_{Se} ~2.8	—
	MBE[70]	V_{Se} ~5.1	—
	Exfoliated[142]	V_{total} ~1.2	—
	Exfoliated[70]	V_{Se} ~8.8	—
	Exfoliated[71]	V_{Se} ~39	3.0
	H_2Se-annealing treated[80]	V_{total} ~0.8	30
$MoSe_2$	CVT[137]	V_{total} >10	—
	Post-annealing treated[137]	V_{total} ~2.5	—

PVD, physical vapour deposition; PLD, pulsed laser deposition; MOCVD, metal–organic CVD; MBE, molecular beam epitaxy; CVT, chemical vapour transport; V_{total}, total point defects; V_S, sulphur vacancies; V_{an}, antisite defects; V_{Se}, selenium vacancies.

the defect sites using a scanning tunnelling microscopy tip, has opened new avenues for atomic-level defect repair[81].

In addition to addressing point defects, it is necessary to eliminate wrinkles in ultraflat 2D single crystals. Wrinkles frequently appear in the as-grown 2D layers upon cooling to room temperature, serving as an effective path to release the compressive strain induced by the mismatch in the thermal expansion coefficients between the 2D materials and their substrates[82]. Unfortunately, wrinkles are considered a kind of line defect that may cause inhomogeneity and reduce electrical mobility and thermal conductivity in large-scale films[83]. Several approaches to synthesizing wrinkle-free ultraflat graphene films, including low-temperature growth[84], using low-thermal-expansion-coefficient substrates[46] or strain-engineered substrates[49], and reducing the interaction between graphene and substrates[85], have been reported.

The quality of monoelemental materials such as graphene has now reached an exceptional level for use in 2D electronic devices. In contrast, multielement 2D compounds tend to demonstrate a higher defect density, primarily attributed to the intricacies involved in supplying multiple precursors. The defect levels of typical 2D vdW materials obtained via different synthesis routes are summarized in Table 1. Ongoing quality control research for these materials is essential for their transition from laboratory to industrial applications, with a basic requirement for the defect densities of 2D-material wafers to be approximately 10^{11} cm^{-2}; at this density, the mobility is considered to be inherently limited by intrinsic phonons[86].

Fabrication of out-of-plane homostructures

Fabrication of homogeneous multilayers

Given the well established monolayer growth techniques, it is reasonable to propose that homogeneous multilayers can be fabricated directly through monolayer epitaxy layer by layer. However, the catalysis or proximity effect is significantly passivated once the substrate surface is entirely covered by monolayers, hindering the nucleation and subsequent growth of adlayers[87]. Meanwhile, strong in-plane covalent bonding and weak out-of-plane vdW interactions lead to preferential in-plane growth. Therefore, activating the nucleation of adlayers and getting rid of vertical epitaxy restrictions are key factors in overcoming this dilemma in multilayer growth.

One straightforward approach to enhancing the nucleation probability of adlayers is feeding ample sources in the layer-by-layer surface epitaxy route (Fig. 4a, top panel). However, it is impractical to infinitely increase the precursor supply. The critical window of source supply needs to maintain a balance between the monolayer full coverage and adlayer nucleation. Early studies have explored several strategies, such as replacing precursor types[88,89], providing higher substrate catalytic activity[90,91], controlling partial pressures[87,92] and adjusting cooling rates[93], to promote the nucleation of the upper adlayers. Apart from the on-top adlayer growth, sources can also squeeze into the interface between the initial layer and the substrate, facilitating the nucleation of the underlying adlayers of graphene[94,95]. Likewise, hBN adlayers are typically formed beneath pre-existing hBN layers, as nitrogen feeding undergoes a surface catalysis process while boron is supplied through surface diffusion or precipitation from the substrate[96]. However, due to the limited source diffusion, achieving a fully covered adlayer beneath existing layers is difficult in the surface epitaxy modes. Moreover, direct multilayer nucleation has been demonstrated to be more thermodynamically favourable on some specially designed epitaxy substrates (Fig. 4a, bottom panel). Six-step terraces on *c*-plane sapphire have been engineered to match the height of bilayer MoS_2, enabling uniform edge nucleation and ultimately coalescence into continuous centimetre-scale bilayers[97] (Fig. 4b). Similarly edge-aligned nucleation has also been reported in the epitaxy of trilayer hBN single crystals on stepped Ni(111) surfaces[98]. Recently, a special bevel-edge structure consisting of Ni(100) and Ni(110) has been designed to fabricate single-crystal rhombohedral boron nitride (rBN) layers with exact interlayer ABC stacking[14].

A surface segregation strategy involving the preimplantation of a large number of source atoms into growth substrates could lead to layer-by-layer segregation of high-coverage adlayers from the substrate surface and the formation of uniform multilayers (Fig. 4c). Typically, the adlayer precipitates underneath the first layer, as verified by isotope-labelling results[99] (Fig. 4d). The source solubility of substrates has great importance for the controlled synthesis of multilayers in this segregation strategy. For instance, transition metals displaying suitable carbon solubilities, such as Ni[100], Ru[101] and alloys of Cu–Ni[102,103], Pt–Si[99] and Cu–Si[104], have been employed to powerfully facilitate the growth of high-coverage multilayer graphene.

Although the surface segregation method can somewhat overcome vertical epitaxy restrictions and enable the fabrication of multilayers, the initiation of thicker layer growth remains unattainable due to the necessity of large-capacity source reservoirs for such thick layers. The dissolution–precipitation method, which utilizes high-solubility substrates to predissolve adequate source atoms, is well demonstrated to be robust in sustaining the precipitation of thick layers after a cooling process (Fig. 4e). Considering the typically proportional relationship between the temperature and solubility, raising the annealing temperature or slowing down the cooling rate is feasible to increase the layer number[105,106]. To further access the maximum solubility,

https://doi.org/10.1038/s41565-024-01704-3

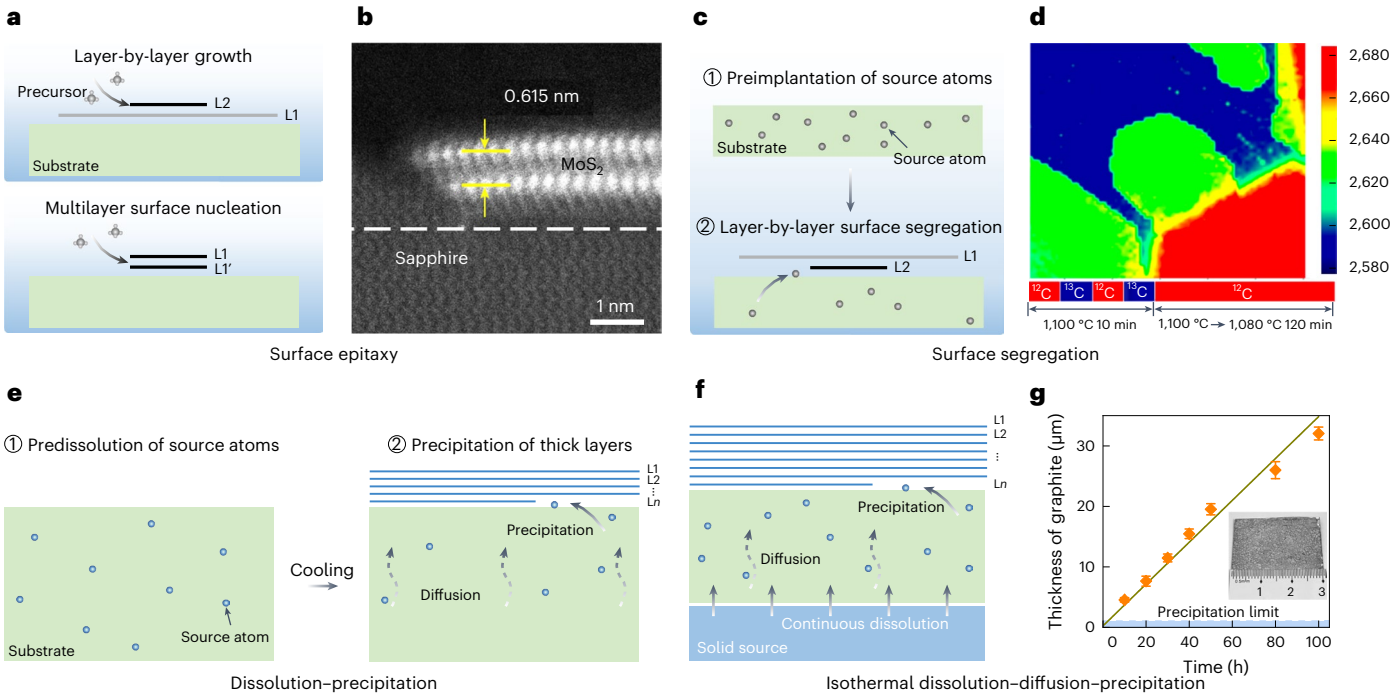

Fig. 4 | Fabrication of homogeneous multilayers. a, Schematic of the surface epitaxy of 2D multilayers, including layer-by-layer growth and multilayer surface nucleation methods. In layer-by-layer growth, new adlayers are grown on top of pre-existing layers, while multilayers nucleate at the same site and grow simultaneously in the multilayer surface nucleation method. **b**, Cross-sectional scanning transmission electron microscopy image of bilayer MoS_2, which simultaneously nucleates on a sapphire substrate. **c**, Schematic for the surface segregation of 2D multilayers; here new adlayers are segregated layer by layer from the substrate and grown underneath the pre-existing layers. **d**, Isotopically labelled Raman map of bilayer graphene, demonstrating that the adlayer is precipitated underneath the first layer on the substrate. **e**, Schematic of dissolution–precipitation growth, which involves predissolution of the source atoms and precipitation of the thick layers upon cooling. **f**, Schematic for isothermal dissolution–diffusion–precipitation growth; this involves a continuous dissolution of a solid source and an isothermal precipitation process. **g**, Thickness evolution with growth time of the epitaxial graphite film produced by the isothermal method. Inset: photograph of the single-crystal epitaxial graphite film. Error bars indicate ± s.d. Panels adapted with permission from: **b**, ref. 97, Springer Nature Limited; **f**,**g**, ref. 109, Springer Nature Limited. Panel **d** reproduced from ref. 99 under a Creative Commons licence CC BY 4.0.

substrates (usually metals, such as Cu, Ni and Fe, and their alloys) can be fully motivated under a molten state by setting an extremely high temperature. Although this dissolution–precipitation method indeed effectively increases the film thickness[107,108], the as-grown films are typically polycrystalline owing to the relatively weak ability of liquid-state metal substrates to modulate domain orientations.

To simultaneously ensure both the crystallinity and thickness of 2D thick films, isothermal dissolution–diffusion–precipitation based on a solid-state single-crystal substrate has been proposed[109] (Fig. 4f). This method involves simultaneous source dissolution and layer precipitation that resemble the filling and release of water in a reservoir, thus surpassing the limitation of inherent solubility and motivating the continuous growth of the ultrathick layers. Moreover, the surface morphology of substrates, such as lattice structure and parallel steps, can be preserved on the solid surface, enabling the unidirectional epitaxy of each monolayer and thus fabricating single-crystal thick films of up to 100,000 layers[109] (Fig. 4g). Utilizing a similar dissolution–diffusion–precipitation method on a vicinal FeNi(111) substrate, rBN crystalline films with parallel stacked layers are controllably synthesized, achieving a high nonlinear optical conversion efficiency of up to 1% (ref. 110).

Increasing the source solubility or ensuring a continuous supply has now enabled us to attain or even surpass the solubility limit, thus successfully extending the fabrication from a few atomic layers to thick crystalline 2D films. Nevertheless, the coverage, uniformity and quality of 2D multilayers still need further optimization.

Fabrication of twisted homostructures

The freedom of twist angles between adjacent layers in 2D materials has given rise to numerous intriguing physical properties. For example, bilayer graphene twisted at 1.1° exhibits flat bands with correlated insulating states[111] and unconventional superconductivity[112], while at 30° it behaves as a quasicrystal with anomalous interlayer electronic coupling[113]. In the twisted TMDC configuration, 3.7°-twisted $MoTe_2$ shows both integer and fractional quantum anomalous Hall states[114], and twisted WSe_2 features low-energy flat bands leading to strongly correlated electronic phases[115]. These twisted homostructures have demonstrated promising applications in the fields of optoelectronics and twistronics[116,117].

Generally, artificial twisted structures with customizable angles can be created by stacking different monolayers using standard transfer techniques or folding methods[118,119]. However, these approaches always suffer from small sizes, interlayer contamination and low throughput. In contrast, the direct growth strategy provides the benefits of large-scale high-quality layers with pristine interfaces, but lacks flexibility in arbitrary twist-angle design. This limitation primarily stems from the high nucleation probability for energetically favourable well stacked bilayers or multilayers, which conversely leads to a low probability for twisted structures. To address this challenge, numerous efforts have been devoted to refining the control of twist angles, evolving from random occurrences to a more controlled process.

The nucleation of adlayers typically occurs at sites with high surface energy on substrates, which commonly share the same nucleation centre as the initial layer[120]. These two monolayers tend to stack in the AB-stacking configuration without interlayer twists since this is a stable structure that minimizes the overlap of $2p_z$ orbitals among different layers[121]. The 30°-twisted bilayer graphene is also frequently observed because this energy-favourable state can be stabilized by the coupling between its armchair edges and the substrate steps[122]

https://doi.org/10.1038/s41565-024-01704-3

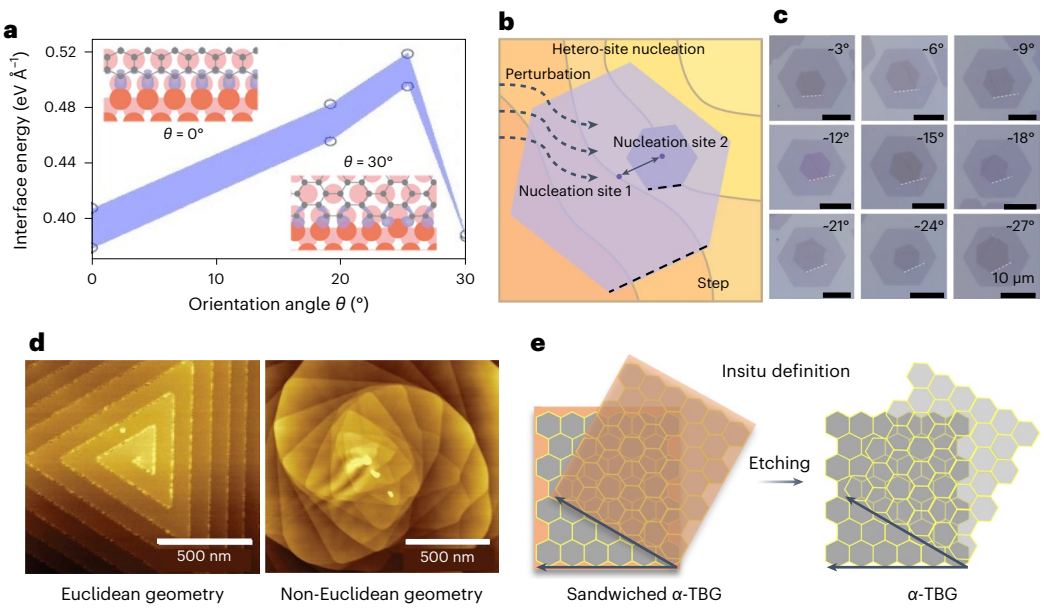

Fig. 5 | Fabrication of twisted homostructures. a, Plot of the interface energy versus the orientation angle of graphene for the homo-site nucleation, showing two preferred orientations at 0° and 30°. **b**, Schematic for the hetero-site nucleation, where the two layers nucleate at different sites and grow independently. **c**, Images of the twisted bilayer graphene (TBG) with different twist angles grown through the hetero-site nucleation initiated by gas-flow perturbation. **d**, Atomic force microscopy images of WS_2 spirals grown on flat (left) and curved (right) substrates. **e**, Schematic for the in situ definition growth of twisted bilayer graphene; here the twist angle is customized during growth. Figure adapted with permission from: **a**, ref. 122, Wiley; **b**,**c**, ref. 126 under a Creative Commons licence CC BY 4.0; **d**, ref. 129, AAAS; **e**, ref. 12, Springer Nature Limited.

(Fig. 5a). Moreover, by controlling the thermodynamic nucleation process and kinetic growth process, or utilizing a sacrificial hBN layer, the morphology and probability of 30°-twisted bilayers can be tailored to some extent[123,124]. Nevertheless, this homo-site growth method occasionally yields a small proportion of random-twist-angle bilayers as by-products[125].

In contrast to the homo-site nucleation growth strategy, the hetero-site nucleation strategy enables each monolayer to nucleate independently at different sites, thereby promoting the efficient formation of twisted bilayers with diverse twist angles (Fig. 5b). Hetero-site nucleation can be initiated by introducing a perturbation during the growth procedure. For example, by involving a gas flow variation[126], a plasma exposure treatment[127] or external ion implantation[128], the fraction of the bilayers with random twist angles can be efficiently increased (Fig. 5c). Although hetero-site nucleation methods have greatly expanded the variety of twist angles, the direct production of on-demand twisted structure still relies on chance occurrences and has not yet reached controllable levels.

Currently, large-scale twisted homostructures with precisely controlled rotation angles can be readily acquired through a transfer procedure following the completion of wafer-scale monolayer growth[11]. In fact, the in situ definition of the twist angles during growth represents the most straightforward way to produce on-demand twisted films. Interlayer twist angles in 2D supertwisted spirals have been introduced with the assistance of screw dislocations and can be tuned by varying the substrate non-planarity. For example, WS_2 spiral growth on a flat substrate (Euclidean geometry) results in aligned layers without interlayer twisting, while supertwisted spirals are constructed on curved substrates via a non-Euclidean twist mechanism[129] (Fig. 5d). Other twisted structures, such as spiral or onion-like morphologies of 2D layers and crystals, have also been sequentially observed, showing the potential for controlling twist angles during growth, but full controllability has yet to be achieved[130–132]. Spiral growth of graphene multilayers through a origami–kirigami approach converts the chirality of a 1D wrinkle into tunable twisted bilayers[133].

An angle replication method has been developed to directly grow twisted bilayer graphene with on-demand angles, which stands as a representative study within the context of in situ definition strategies[12] (Fig. 5e). The twist angle is completely duplicated from the rotation of the prestacked substrates and is locked by the strong interaction between the graphene and the substrate, thereby preventing slippage towards an energy-minimal angle and enabling the achievement of small twist angles such as 1°.

In summary, both homo-site and hetero-site nucleation growth are capable of producing twisted homostructures, but their effectiveness mostly depends on the probability of nucleation at random angles. Meanwhile, the concept of directly growing twisted layers with predesigned twist angles has been initially validated but is still in a preliminary stage.

Conclusions and perspectives

Over the past decade, remarkable strides have been made in the epitaxial growth of 2D vdW materials, evolving from in-plane single-crystal monolayers to out-of-plane multilayer structures. The fabrication of some typical materials has now reached an advanced stage, with achievements such as the industrial-scale production of graphene single-crystal films, inch-sized synthesis of hBN single-crystal monolayers, and TMDC semiconductors reaching standard wafer sizes up to 300 mm that align with mainstream silicon technology[134]. In addition, the epitaxy of multilayers with parallel stacking or precise control of the twist angles in homostructures has made some stagewise progress. We have summarized the strategies underlying these cases in this Review and believe that they could be further extended to other epitaxy techniques or 2D systems as well. The single-crystal epitaxy of complex vdW compounds such as metal oxides or hydroxides is in an exploratory stage following these established strategies. Although this Review does not discuss non-vdW layered or non-layered systems, certain principles may inspire research in the in-plane nucleation and orientation control of these systems, broadening our current comprehension of 2D materials.

Extensive data and device prototypes reveal the promising application potential of 2D materials. However, the crystalline quality, composition controllability and production yield of the current 2D layers are still far from the manufacturing readiness of conventional semiconductor technology. A challenge in the development of 2D semiconductors is their excessive defect density (typically 10^{12}–10^{13} cm^{-2}), which is orders of magnitude greater than that in epitaxial III–V semiconductor films. Innovative strategies for atomic-level composition control are urgently needed to achieve the synthesis of stoichiometric single crystals and enable precise doping or alloying to tailor their electrical, optical and magnetic properties. Direct synthesis or fine-tuned doping of the p-type 2D semiconductors necessitates further efforts to realize the logic function of complementary metal oxide semiconductors in 2D electronics. Moreover, quantitative characterization methods for defects, crystallinity, doping levels and structural phases need to be correspondingly developed, along with the establishment of a self-contained and standardized process, to ensure the quality and reliability of 2D materials as candidates in the semiconductor industry.

The functionalization and on-demand customization of 2D materials are imperative for satisfying specific application requirements. Exploring the fabrication of homogeneous multilayers and novel architectures with various 2D materials unveils exciting opportunities. For instance, uniform thin layers exhibit enhanced mobility and improved dielectric shielding effects, potentially meeting the requirements for transistor channel materials to combine ultimate electrostatic control and sufficient drive current. More than Moore applications, such as micro- and nanoelectromechanical systems, pose a demand for the preparation of 2D membranes with controllable thickness and high intralayer crystallinity to exhibit exceptional mechanical properties and high sensitivity to vibrations and piezoresistance. Meanwhile, it is time now to create a database to provide a systematic overview of the properties of known materials or hybrid structures, and establish the relationship among the processes, structures, performance and applications through machine learning. This database would offer researchers rational approaches to designing functions of 2D architectures through configuration manufacturing, opening up new possibilities for the next-generation 2D-material-based devices.

In device application scenarios, 2D architectures should ideally be initiated and formed during the material fabrication processes. Advanced techniques for the direct growth or wafer-scale transfer of 2D films on insulating wafers are crucial for incorporating 2D field-effect transistors into future very large-scale integration devices. Affordable thermal budget solutions need to be devised for material growth and subsequent device manufacturing to be compatible with back-end-of-line processes. The next step is to bridge the industrial chain from material design to packaging and device integration. Ultimately, once the growth readiness level and production reproducibility of 2D materials reach parity with silicon wafers, their transition from research (lab) to design and manufacture (fab) will be around the corner.

References

1. Mounet, N. et al. Two-dimensional materials from high-throughput computational exfoliation of experimentally known compounds. *Nat. Nanotechnol.* **13**, 246–252 (2018).
2. May, J. W. Platinum surface LEED rings. *Surf. Sci.* **17**, 267–270 (1969).
3. Koma, A., Sunouchi, K. & Miyajima, T. Fabrication and characterization of heterostructures with subnanometer thickness. *Microelectron. Eng.* **2**, 129–136 (1984).
4. Li, X. et al. Large-area synthesis of high-quality and uniform graphene films on copper foils. *Science* **324**, 1312–1314 (2009).
   This study synthesizes centimetre-scale high-quality graphene films on Cu substrates via CVD using methane.
5. Bae, S. et al. Roll-to-roll production of 30-inch graphene films for transparent electrodes. *Nat. Nanotechnol.* **5**, 574–578 (2010).
6. Xu, X. Z. et al. Ultrafast epitaxial growth of metre-sized single-crystal graphene on industrial Cu foil. *Sci. Bull.* **62**, 1074–1080 (2017).
7. Wang, L. et al. Epitaxial growth of a 100-square-centimetre single-crystal hexagonal boron nitride monolayer on copper. *Nature* **570**, 91–95 (2019).
   This study demonstrates the growth of decimetre-scale single-crystal hBN monolayers via a step-edge-guided unidirectional nucleation.
8. Liu, C., Wang, L., Qi, J. & Liu, K. Designed growth of large-size 2D single crystals. *Adv. Mater.* **32**, 2000046 (2020).
9. Li, T. T. et al. Epitaxial growth of wafer-scale molybdenum disulfide semiconductor single crystals on sapphire. *Nat. Nanotechnol.* **16**, 1201–1207 (2021).
10. Xu, X. et al. Seeded 2D epitaxy of large-area single-crystal films of the van der Waals semiconductor 2H $MoTe_2$. *Science* **372**, 195–200 (2021).
    This work reports a seeded epitaxy of wafer-scale single-crystal 2H-$MoTe_2$ that triggered from an implanted 2H-$MoTe_2$ single seed crystal.
11. Liao, M. Z. et al. Precise control of the interlayer twist angle in large scale MoS_2 homostructures. *Nat. Commun.* **11**, 2153 (2020).
12. Liu, C. et al. Designed growth of large bilayer graphene with arbitrary twist angles. *Nat. Mater.* **21**, 1263–1268 (2022).
13. Du, L. et al. Moiré photonics and optoelectronics. *Science* **379**, eadg0014 (2023).
14. Wang, L. et al. Bevel-edge epitaxy of ferroelectric rhombohedral boron nitride single crystal. *Nature* **629**, 74–79 (2024).
15. Wu, R. et al. Large-area single-crystal sheets of borophene on Cu(111) surfaces. *Nat. Nanotechnol.* **14**, 44–49 (2019).
16. Chen, C. et al. Growth of single-crystal black phosphorus and its alloy films through sustained feedstock release. *Nat. Mater.* **22**, 717–724 (2023).
17. Zhou, Z. et al. Low symmetric sub-wavelength array enhanced lensless polarization-sensitivity photodetector of germanium selenium. *Sci. Bull.* **68**, 173–179 (2023).
18. Lin, Y.-C. et al. Recent advances in 2D material theory, synthesis, properties, and applications. *ACS Nano* **17**, 9694–9747 (2023).
19. Braeuninger-Weimer, P., Brennan, B., Pollard, A. J. & Hofmann, S. Understanding and controlling Cu-catalyzed graphene nucleation: the role of impurities, roughness, and oxygen scavenging. *Chem. Mater.* **28**, 8905–8915 (2016).
20. Yan, Z. et al. Toward the synthesis of wafer-scale single-crystal graphene on copper foils. *ACS Nano* **6**, 9110–9117 (2012).
21. Sridhara, K. et al. Electrochemically prepared polycrystalline copper surface for the growth of hexagonal boron nitride. *Cryst. Growth Des.* **17**, 1669–1678 (2017).
22. Wang, H. et al. Controllable synthesis of submillimeter single-crystal monolayer graphene domains on copper foils by suppressing nucleation. *J. Am. Chem. Soc.* **134**, 3627–3630 (2012).
23. Wang, L. et al. Monolayer hexagonal boron nitride films with large domain size and clean interface for enhancing the mobility of graphene-based field-effect transistors. *Adv. Mater.* **26**, 1559–1564 (2014).
24. Li, X. et al. Large-area graphene single crystals grown by low-pressure chemical vapor deposition of methane on copper. *J. Am. Chem. Soc.* **133**, 2816–2819 (2011).
25. Ji, Y. et al. Chemical vapor deposition growth of large single-crystal mono-, bi-, tri-layer hexagonal boron nitride and their interlayer stacking. *ACS Nano* **11**, 12057–12066 (2017).
26. Chen, J. et al. Chemical vapor deposition of large-size monolayer $MoSe_2$ crystals on molten glass. *J. Am. Chem. Soc.* **139**, 1073–1076 (2017).

27. Lee, J. S. et al. Wafer-scale single-crystal hexagonal boron nitride film via self-collimated grain formation. *Science* **362**, 817–821 (2018).
28. Hao, Y. et al. The role of surface oxygen in the growth of large single-crystal graphene on copper. *Science* **342**, 720–723 (2013).
29. Lin, L. et al. Surface engineering of copper foils for growing centimeter-sized single-crystalline graphene. *ACS Nano* **10**, 2922–2929 (2016).
30. Wang, H. et al. Primary nucleation-dominated chemical vapor deposition growth for uniform graphene monolayers on dielectric substrate. *J. Am. Chem. Soc.* **141**, 11004–11008 (2019).
31. Ma, T. et al. Repeated growth–etching–regrowth for large-area defect-free single-crystal graphene by chemical vapor deposition. *ACS Nano* **8**, 12806–12813 (2014).
32. Wang, L. et al. Water-assisted growth of large-sized single crystal hexagonal boron nitride grains. *Mater. Chem. Front.* **1**, 1836–1840 (2017).
33. Chen, W. et al. Oxygen-assisted chemical vapor deposition growth of large single-crystal and high-quality monolayer MoS_2. *J. Am. Chem. Soc.* **137**, 15632–15635 (2015).
34. Gong, Y. et al. Synthesis of millimeter-scale transition metal dichalcogenides single crystals. *Adv. Funct. Mater.* **26**, 2009–2015 (2016).
35. Lim, Y.-F. et al. Modification of vapor phase concentrations in MoS_2 growth using a NiO foam barrier. *ACS Nano* **12**, 1339–1349 (2018).
36. Suzuki, H. et al. Surface diffusion-limited growth of large and high-quality monolayer transition metal dichalcogenides in confined space of microreactor. *ACS Nano* **16**, 11360–11373 (2022).
37. Chang, M.-C. et al. Fast growth of large-grain and continuous MoS_2 films through a self-capping vapor–liquid–solid method. *Nat. Commun.* **11**, 3682 (2020).
38. Wu, T. R. et al. Fast growth of inch-sized single-crystalline graphene from a controlled single nucleus on Cu–Ni alloys. *Nat. Mater.* **15**, 43–47 (2016).
This work presents a local feeding technique to control the nucleation of a single graphene nucleus, enabling the evolution into an inch-sized single-crystal domain.
39. Vlassiouk, I. V. et al. Evolutionary selection growth of two-dimensional materials on polycrystalline substrates. *Nat. Mater.* **17**, 318–322 (2018).
40. Xing, S., Wu, W., Wang, Y., Bao, J. & Pei, S.-S. Kinetic study of graphene growth: temperature perspective on growth rate and film thickness by chemical vapor deposition. *Chem. Phys. Lett.* **580**, 62–66 (2013).
41. Liu, C. et al. Kinetic modulation of graphene growth by fluorine through spatially confined decomposition of metal fluorides. *Nat. Chem.* **11**, 730–736 (2019).
42. Huang, P. Y. et al. Grains and grain boundaries in single-layer graphene atomic patchwork quilts. *Nature* **469**, 389–392 (2011).
43. Gao, L., Guest, J. R. & Guisinger, N. P. Epitaxial graphene on Cu(111). *Nano Lett.* **10**, 3512–3516 (2010).
44. Murdock, A. T. et al. Controlling the orientation, edge geometry, and thickness of chemical vapor deposition graphene. *ACS Nano* **7**, 1351–1359 (2013).
45. Nguyen, V. L. et al. Seamless stitching of graphene domains on polished copper (111) foil. *Adv. Mater.* **27**, 1376–1382 (2015).
46. Lee, J. H. et al. Wafer-scale growth of single-crystal monolayer graphene on reusable hydrogen-terminated germanium. *Science* **344**, 286–289 (2014).
This study demonstrates wafer-scale single-crystal graphene grown on H–Ge(110) through seamless merging of multiple unidirectionally aligned domains.
47. Jin, S. et al. Colossal grain growth yields single-crystal metal foils by contact-free annealing. *Science* **362**, 1021–1025 (2018).
48. Nguyen, V. L. et al. Wafer-scale single-crystalline AB-stacked bilayer graphene. *Adv. Mater.* **28**, 8177–8183 (2016).
49. Deng, B. et al. Wrinkle-free single-crystal graphene wafer grown on strain-engineered substrates. *ACS Nano* **11**, 12337–12345 (2017).
50. Song, X. J. et al. Chemical vapor deposition growth of large-scale hexagonal boron nitride with controllable orientation. *Nano Res.* **8**, 3164–3176 (2015).
51. Yu, H. et al. Wafer-scale growth and transfer of highly-oriented monolayer MoS_2 continuous films. *ACS Nano* **11**, 12001–12007 (2017).
52. Li, J. D. et al. Growth of polar hexagonal boron nitride monolayer on nonpolar copper with unique orientation. *Small* **12**, 3645–3650 (2016).
53. Cuccureddu, F. et al. Surface morphology of *c*-plane sapphire (α-alumina) produced by high temperature anneal. *Surf. Sci.* **604**, 1294–1299 (2010).
54. Fu, J.-H. et al. Oriented lateral growth of two-dimensional materials on *c*-plane sapphire. *Nat. Nanotechnol.* **18**, 1289–1294 (2023).
55. Chen, T. A. et al. Wafer-scale single-crystal hexagonal boron nitride monolayers on Cu(111). *Nature* **579**, 219–223 (2020).
56. Yang, P. F. et al. Epitaxial growth of centimeter-scale single-crystal MoS_2 monolayer on Au(111). *ACS Nano* **14**, 5036–5045 (2020).
57. Wang, J. H. et al. Dual-coupling-guided epitaxial growth of wafer-scale single-crystal WS_2 monolayer on vicinal *a*-plane sapphire. *Nat. Nanotechnol.* **17**, 33–38 (2022).
58. Yang, P. et al. Highly reproducible epitaxial growth of wafer-scale single-crystal monolayer MoS_2 on sapphire. *Small Methods* **7**, 2300165 (2023).
59. Zhou, X. et al. Step-climbing epitaxy of layered materials with giant out-of-plane lattice mismatch. *Adv. Mater.* **34**, 2202754 (2022).
60. Arias, P., Ebnonnasir, A., Ciobanu, C. V. & Kodambaka, S. Growth kinetics of two-dimensional hexagonal boron nitride layers on Pd(111). *Nano Lett.* **20**, 2886–2891 (2020).
61. Zheng, P. et al. Universal epitaxy of non-centrosymmetric two-dimensional single-crystal metal dichalcogenides. *Nat. Commun.* **14**, 592 (2023).
62. Zhu, H. et al. Step engineering for nucleation and domain orientation control in WSe_2 epitaxy on *c*-plane sapphire. *Nat. Nanotechnol.* **18**, 1295–1302 (2023).
63. Xu, X. et al. Growth of 2D materials at the wafer scale. *Adv. Mater.* **34**, 2108258 (2022).
64. Cai, Z., Liu, B., Zou, X. & Cheng, H.-M. Chemical vapor deposition growth and applications of two-dimensional materials and their heterostructures. *Chem. Rev.* **118**, 6091–6133 (2018).
65. Wang, M. et al. Single-crystal, large-area, fold-free monolayer graphene. *Nature* **596**, 519–524 (2021).
66. Wang, L. et al. One-dimensional electrical contact to a two-dimensional material. *Science* **342**, 614–617 (2013).
67. Hong, J. et al. Exploring atomic defects in molybdenum disulphide monolayers. *Nat. Commun.* **6**, 6293 (2015).
68. Vancsó, P. et al. The intrinsic defect structure of exfoliated MoS_2 single layers revealed by scanning tunneling microscopy. *Sci. Rep.* **6**, 29726 (2016).
69. Wang, S., Robertson, A. & Warner, J. H. Atomic structure of defects and dopants in 2D layered transition metal dichalcogenides. *Chem. Soc. Rev.* **47**, 6764–6794 (2018).
70. Ding, S., Lin, F. & Jin, C. Quantify point defects in monolayer tungsten diselenide. *Nanotechnology* **32**, 255701 (2021).
71. Choi, S. H. et al. Is chemical vapor deposition of monolayer WSe_2 comparable to other synthetic routes? *APL Mater.* **11**, 111124 (2023).

72. Feng, S. et al. Synthesis of ultrahigh-quality monolayer molybdenum disulfide through in situ defect healing with thiol molecules. *Small* **16**, 2003357 (2020).
73. Wan, Y. et al. Low-defect-density WS_2 by hydroxide vapor phase deposition. *Nat. Commun.* **13**, 4149 (2022).
74. Zuo, Y. G. et al. Robust growth of two-dimensional metal dichalcogenides and their alloys by active chalcogen monomer supply. *Nat. Commun.* **13**, 1007 (2022).
75. Xue, G. et al. Modularized batch production of 12-inch transition metal dichalcogenides by local element supply. *Sci. Bull.* **68**, 1514–1521 (2023).
This work develops a modularized local-element-supply strategy, achieving batch production of TMDC wafers up to 12 inches.
76. Shen, Y. et al. In situ repair of 2D chalcogenides under electron beam irradiation. *Adv. Mater.* **30**, 1705954 (2018).
77. Xu, X. et al. Atomic-precision repair of a few-layer 2H-$MoTe_2$ thin film by phase transition and recrystallization induced by a heterophase interface. *Adv. Mater.* **32**, 2000236 (2020).
78. López, V. et al. Chemical vapor deposition repair of graphene oxide: a route to highly-conductive graphene monolayers. *Adv. Mater.* **21**, 4683–4686 (2009).
79. Yu, Z. et al. Towards intrinsic charge transport in monolayer molybdenum disulfide by defect and interface engineering. *Nat. Commun.* **5**, 5290 (2014).
80. Lin, Y.-C. et al. Realizing large-scale, electronic-grade two-dimensional semiconductors. *ACS Nano* **12**, 965–975 (2018).
81. Gurlu, O. et al. Controlled damaging and repair of self-organized nanostructures by atom manipulation at room temperature. *Nanotechnology* **18**, 365305 (2007).
82. Chae, S. J. et al. Synthesis of large-area graphene layers on poly-nickel substrate by chemical vapor deposition: wrinkle formation. *Adv. Mater.* **21**, 2328–2333 (2009).
83. Zhu, W. et al. Structure and electronic transport in graphene wrinkles. *Nano Lett.* **12**, 3431–3436 (2012).
84. Gao, L. B. et al. Face-to-face transfer of wafer-scale graphene films. *Nature* **505**, 190–194 (2014).
85. Yuan, G. et al. Proton-assisted growth of ultraflat graphene films. *Nature* **577**, 204–208 (2020).
86. Das, S. et al. Transistors based on two-dimensional materials for future integrated circuits. *Nat. Electron.* **4**, 786–799 (2021).
87. Zhou, H. L. et al. Chemical vapour deposition growth of large single crystals of monolayer and bilayer graphene. *Nat. Commun.* **4**, 2096 (2013).
88. Sun, Z. Z. et al. Growth of graphene from solid carbon sources. *Nature* **468**, 549–552 (2010).
89. Wassei, J. K. et al. Chemical vapor deposition of graphene on copper from methane, ethane and propane: evidence for bilayer selectivity. *Small* **8**, 1415–1422 (2012).
90. Yan, K., Peng, H. L., Zhou, Y., Li, H. & Liu, Z. F. Formation of bilayer Bernal graphene: layer-by-layer epitaxy via chemical vapor deposition. *Nano Lett.* **11**, 1106–1110 (2011).
91. Zhang, Z. et al. Layer-by-layer growth of bilayer graphene single-crystals enabled by self-transmitting catalytic activity. Preprint at https://arxiv.org/abs/2205.01468 (2022).
92. Zhao, M. et al. Enhanced copper anticorrosion from Janus-doped bilayer graphene. *Nat. Commun.* **14**, 7447 (2023).
93. Lee, S., Lee, K. & Zhong, Z. H. Wafer scale homogeneous bilayer graphene films by chemical vapor deposition. *Nano Lett.* **10**, 4702–4707 (2010).
94. Li, Q. Y. et al. Growth of adlayer graphene on Cu studied by carbon isotope labeling. *Nano Lett.* **13**, 486–490 (2013).
95. Zhang, X. Y., Wang, L., Xin, J., Yakobson, B. I. & Ding, F. Role of hydrogen in graphene chemical vapor deposition growth on a copper surface. *J. Am. Chem. Soc.* **136**, 3040–3047 (2014).
96. Kidambi, P. R. et al. In situ observations during chemical vapor deposition of hexagonal boron nitride on polycrystalline copper. *Chem. Mater.* **26**, 6380–6392 (2014).
97. Liu, L. et al. Uniform nucleation and epitaxy of bilayer molybdenum disulfide on sapphire. *Nature* **605**, 69–75 (2002).
This study reports the synthesis of centimetre-scale MoS_2 bilayers by engineering the atomic terrace height on c-plane sapphire to enable an edge-nucleation mechanism.
98. Ma, K. Y. et al. Epitaxial single-crystal hexagonal boron nitride multilayers on Ni(111). *Nature* **606**, 88–93 (2022).
This study presents the edge-aligned nucleation of trilayer hBN domains on stepped Ni(111) surfaces, realizing the epitaxial growth of wafer-scale single-crystal hBN trilayers.
99. Ma, W. et al. Interlayer epitaxy of wafer-scale high-quality uniform AB-stacked bilayer graphene films on liquid Pt_3Si/solid Pt. *Nat. Commun.* **10**, 2809 (2019).
100. Reina, A. et al. Growth of large-area single- and bi-layer graphene by controlled carbon precipitation on polycrystalline Ni surfaces. *Nano Res.* **2**, 509–516 (2009).
101. Sutter, P. W., Flege, J. I. & Sutter, E. A. Epitaxial graphene on ruthenium. *Nat. Mater.* **7**, 406–411 (2008).
102. Takesaki, Y. et al. Highly uniform bilayer graphene on epitaxial Cu–Ni(111) alloy. *Chem. Mater.* **28**, 4583–4592 (2016).
103. Huang, M. et al. Large-area single-crystal AB-bilayer and ABA-trilayer graphene grown on a Cu/Ni(111) foil. *Nat. Nanotechnol.* **15**, 289–295 (2020).
104. Nguyen, V. L. et al. Layer-controlled single-crystalline graphene film with stacking order via Cu–Si alloy formation. *Nat. Nanotechnol.* **15**, 861–867 (2020).
105. Zhang, L., Dong, J. & Ding, F. Strategies, status, and challenges in wafer scale single crystalline two-dimensional materials synthesis. *Chem. Rev.* **121**, 6321–6372 (2021).
106. Qiu, W. et al. Thickness-controlled growth of multilayer graphene on Ni(111) using an approximate equilibrium segregation method for applications in spintronic devices. *ACS Appl. Nano Mater.* **6**, 4236–4242 (2023).
107. Shi, Z. Y. et al. Vapor–liquid–solid growth of large-area multilayer hexagonal boron nitride on dielectric substrates. *Nat. Commun.* **11**, 849 (2020).
108. Li, Y. F. et al. Synthesis of centimeter-scale high-quality polycrystalline hexagonal boron nitride films from Fe fluxes. *Nanoscale* **13**, 11223–11231 (2021).
109. Zhang, Z. B. et al. Continuous epitaxy of single-crystal graphite films by isothermal carbon diffusion through nickel. *Nat. Nanotechnol.* **17**, 1258–1264 (2022).
110. Qi, J. et al. Stacking-controlled growth of rBN crystalline films with high nonlinear optical conversion efficiency up to 1%. *Adv. Mater.* **36**, 2303122 (2024).
111. Cao, Y. et al. Correlated insulator behaviour at half-filling in magic-angle graphene superlattices. *Nature* **556**, 80–84 (2018).
112. Cao, Y. et al. Unconventional superconductivity in magic-angle graphene superlattices. *Nature* **556**, 43–50 (2018).
113. Ahn, S. J. et al. Dirac electrons in a dodecagonal graphene quasicrystal. *Science* **361**, 782–786 (2018).
114. Park, H. et al. Observation of fractionally quantized anomalous Hall effect. *Nature* **622**, 74–79 (2023).
115. Wang, L. et al. Correlated electronic phases in twisted bilayer transition metal dichalcogenides. *Nat. Mater.* **19**, 861–866 (2020).
116. Ciarrocchi, A., Tagarelli, F., Avsar, A. & Kis, A. Excitonic devices with van der Waals heterostructures: valleytronics meets twistronics. *Nat. Rev. Mater.* **7**, 449–464 (2022).
117. Xin, K., Wang, X., Grove-Rasmussen, K. & Wei, Z. Twist-angle two-dimensional superlattices and their application in (opto) electronics. *J. Semicond.* **43**, 011001 (2022).

118. Schmidt, H., Rode, J. C., Smirnov, D. & Haug, R. J. Superlattice structures in twisted bilayers of folded graphene. *Nat. Commun.* **5**, 5742 (2014).
119. Ribeiro-Palau, R. et al. Twistable electronics with dynamically rotatable heterostructures. *Science* **361**, 690–693 (2018).
120. Gao, J. F., Yip, J., Zhao, J. J., Yakobson, B. I. & Ding, F. Graphene nucleation on transition metal surface: structure transformation and role of the metal step edge. *J. Am. Chem. Soc.* **133**, 5009–5015 (2011).
121. Wu, Y. P. et al. Growth mechanism and controlled synthesis of AB-stacked bilayer graphene on Cu–Ni alloy foils. *ACS Nano* **6**, 7731–7738 (2012).
122. Yan, Z. et al. Large hexagonal bi- and trilayer graphene single crystals with varied interlayer rotations. *Angew. Chem. Int. Ed.* **53**, 1565–1569 (2014).
123. Pezzini, S. et al. 30 degrees-twisted bilayer graphene quasicrystals from chemical vapor deposition. *Nano Lett.* **20**, 3313–3319 (2020).
124. Deng, B. et al. Interlayer decoupling in 30 degrees twisted bilayer graphene quasicrystal. *ACS Nano* **14**, 1656–1664 (2020).
125. Lu, C. C. et al. Twisting bilayer graphene superlattices. *ACS Nano* **7**, 2587–2594 (2013).
126. Sun, L. Z. et al. Hetero-site nucleation for growing twisted bilayer graphene with a wide range of twist angles. *Nat. Commun.* **12**, 2391 (2021).
127. Chen, Y. C. et al. Direct growth of mm-size twisted bilayer graphene by plasma-enhanced chemical vapor deposition. *Carbon* **156**, 212–224 (2020).
128. Zheng, H. et al. Strong interlayer coupling in twisted transition metal dichalcogenide Moiré superlattices. *Adv. Mater.* **35**, 2210909 (2023).
129. Zhao, Y. et al. Supertwisted spirals of layered materials enabled by growth on non-Euclidean surfaces. *Science* **370**, 442–445 (2020). **This study presents a general model for the growth of layered materials with screw-dislocation spirals on non-Euclidean surfaces, resulting in continuously twisted homostructures.**
130. Zhang, L. M. et al. Three-dimensional spirals of atomic layered MoS_2. *Nano Lett.* **14**, 6418–6423 (2014).
131. Fan, X. P. et al. Controllable growth and formation mechanisms of dislocated WS_2 spirals. *Nano Lett.* **18**, 3885–3892 (2018).
132. Liu, Y. et al. Helical van der Waals crystals with discretized Eshelby twist. *Nature* **570**, 358–362 (2019).
133. Wang, Z.-J. et al. Conversion of chirality to twisting via sequential one-dimensional and two-dimensional growth of graphene spirals. *Nat. Mater.* **23**, 331–338 (2024).
134. Xia, Y. et al. 12-inch growth of uniform MoS_2 monolayer for integrated circuit manufacture. *Nat. Mater.* **22**, 1324–1331 (2023).
135. Malekpour, H. et al. Thermal conductivity of graphene with defects induced by electron beam irradiation. *Nanoscale* **8**, 14608–14616 (2016).
136. Zhong, J.-H. et al. Quantitative correlation between defect density and heterogeneous electron transfer rate of single layer graphene. *J. Am. Chem. Soc.* **136**, 16609–16617 (2014).
137. Edelberg, D. et al. Approaching the intrinsic limit in transition metal diselenides via point defect control. *Nano Lett.* **19**, 4371–4379 (2019).
138. Qiu, H. et al. Hopping transport through defect-induced localized states in molybdenum disulphide. *Nat. Commun.* **4**, 2642 (2013).
139. Bertoldo, F. et al. Intrinsic defects in MoS_2 grown by pulsed laser deposition: from monolayers to bilayers. *ACS Nano* **15**, 2858–2868 (2021).
140. Torsi, R. et al. Dilute rhenium doping and its impact on defects in MoS_2. *ACS Nano* **17**, 15629–15640 (2023).
141. Zhang, Y. et al. Electronic structure, surface doping, and optical response in epitaxial WSe_2 thin films. *Nano Lett.* **16**, 2485–2491 (2016).
142. Addou, R. & Wallace, R. M. Surface analysis of WSe_2 crystals: spatial and electronic variability. *ACS Appl. Mater. Interfaces* **8**, 26400–26406 (2016).
143. Lee, Y. H. et al. Synthesis of large-area MoS_2 atomic layers with chemical vapor deposition. *Adv. Mater.* **24**, 2320–2325 (2012).
144. Kim, K. K. et al. Synthesis of monolayer hexagonal boron nitride on Cu foil using chemical vapor deposition. *Nano Lett.* **12**, 161–166 (2012).
145. Zhu, J. et al. Low-thermal-budget synthesis of monolayer molybdenum disulfide for silicon back-end-of-line integration on a 200 mm platform. *Nat. Nanotechnol.* **18**, 456–463 (2023). **This work reports the low-temperature MOCVD growth for 8-inch MoS_2, facilitating a direct integration of MoS_2 transistors with silicon complementary metal–oxide–semiconductor circuits.**
146. Reina, A. et al. Large area, few-layer graphene films on arbitrary substrates by chemical vapor deposition. *Nano Lett.* **9**, 30–35 (2009).
147. Shi, Y. et al. Synthesis of few-layer hexagonal boron nitride thin film by chemical vapor deposition. *Nano Lett.* **10**, 4134–4139 (2010).
148. Song, L. et al. Large scale growth and characterization of atomic hexagonal boron nitride layers. *Nano Lett.* **10**, 3209–3215 (2010).
149. Wang, X. S., Feng, H. B., Wu, Y. M. & Jiao, L. Y. Controlled synthesis of highly crystalline MoS_2 flakes by chemical vapor deposition. *J. Am. Chem. Soc.* **135**, 5304–5307 (2013).
150. Zhao, P. et al. Equilibrium chemical vapor deposition growth of Bernal-stacked bilayer graphene. *ACS Nano* **8**, 11631–11638 (2014).
151. Uchida, Y. et al. Controlled growth of large-area uniform multilayer hexagonal boron nitride as an effective 2D substrate. *ACS Nano* **12**, 6236–6244 (2018).

Acknowledgements

This work was supported by the National Natural Science Foundation of China (52025023, 52322205, 52250398, 12274456, 51991342, 52021006, 11888101, T2188101), the National Key R&D Program of China (2022YFA1403500 and 2022YFA1405600), Guangdong Major Project of Basic and Applied Basic Research (2021B0301030002), Beijing Municipal Science and Technology Project (Z221100005822003), the Strategic Priority Research Program of Chinese Academy of Sciences (XDB33000000) and the New Cornerstone Science Foundation through the XPLORER PRIZE.

Competing interests

The authors declare no competing interests.

Additional information

Correspondence and requests for materials should be addressed to Kaihui Liu.

Peer review information *Nature Nanotechnology* thanks Po-Wen Chiu and the other, anonymous, reviewer(s) for their contribution to the peer review of this work.